A Comparison Between Numerical Predictions and Theoretical and Experimental Results for Laminar Core-Annular Flow

Jeroen C. Beerens, Gijs Ooms, Mathieu J. B. M. Pourquie, and Jerry Westerweel
J.M. Burgerscentrum, Faculty of Mechanical Engineering, Laboratory for Aero- and Hydrodynamics,
Delft University of Technology, Mekelweg 2, 2628 CD Delft, The Netherlands

DOI 10.1002/aic.14463
Published online April 23, 2014 in Wiley Online Library (wileyonlinelibrary.com)

A numerical study, using the volume-of-fluid method, has been made of vertical (upward) laminar core-annular flow: the flow of a high-viscosity liquid core surrounded by a laminar low-viscosity liquid annular layer through a vertical pipe. The numerical results are compared with theoretical results from linear stability calculations and with experimental data. The comparison is good and the general conclusion of our study is that it is very well possible to simulate laminar core-annular flow in a pipe using the volume-of-fluid method. © 2014 The Authors. AIChE Journal, published by Wiley on behalf of the AIChE. This is an open access article under the terms of the Creative Commons Attribution License, which permits use, distribution and reproduction in any medium, provided the original work is properly cited. *AIChE J*, 60: 3046–3056, 2014
Keywords: vertical laminar core-annular flow, numerical simulation, volume-of-fluid method

Introduction

We study the flow of a high-viscosity liquid surrounded by a low-viscosity liquid through a pipe. This core-annular flow is very interesting from a practical and scientific point of view. Joseph and Renardy[1] have written a book about it. There are several review articles, see for instance Oliemans and Ooms[2] and Joseph et al.[3] A perfect core-annular flow (PCAF) with a smooth interface between the two liquids is not often observed. Usually this interface is wavy due to the growth of instabilities. However, although the interface is wavy, at the correct operating conditions these waves do not grow indefinitely in amplitude due to nonlinear effects. Their shape may change, but the waves remain free from the pipe wall. More details about the results of linear stability calculations for the growth of waves at the interface (and about the effect of interfacial tension) are given by Li and Renardy.[4]

It has been shown that laminar core-annular flow (high-viscosity core, laminar low-viscosity annular layer) can be simulated by means of numerical calculations using the volume-of-fluid method, see Li and Renardy[4] and Ooms et al.[5] In these articles, the validation of the method against theoretical results (of linear stability calculations) and experiments is somewhat limited. Therefore, we have extended this validation significantly for the case of vertical (upward) laminar core-annular flow and the results are presented in this article. Linear stability calculations provide the initial growth of a wave at the core-annular interface, its wavelength and wave speed. Moreover, maps with stable and unstable regions have been developed (see Hu et al.[6]). Experiments have been performed and documented by Bai et al.[7] They give an extensive set of results for pressure drop, slip ratio, and flow patterns as a function of superficial oil and water velocities. We have compared the results of our numerical simulations with these theoretical and experimental results.

From the practical point of view, the motivation for simulating wavy core-annular flow is to examine the effect of the waves on the oil and water flow rates for given pressure drop and average *in situ* volume fraction of oil and water, as compared to the values predicted assuming a smooth interface (for which a simple analytical solution can be used). We will show that this effect is considerable.

Numerical Solution Method

The numerical method used for this investigation is based on the volume-of-fluid solver incorporated in the package OpenFOAM (The OpenFOAM open source toolbox is produced by ESI-OpenCFD and is distributed through the OpenFOAM Foundation. OpenCFD was founded by Henry Weller, Chris Greenshields, and Mattijs Janssens. [For details see: https://github.com/OpenFOAM/OpenFOAM-2.1.x]). The Navier–Stokes equations are solved on a fixed grid. The viscosity and density are nonuniform and calculated via an indicator function. This indicator function is transported through the domain by an advection equation. The version 2.1 of OpenFOAM has been used. The grids were equidistant, orthogonal, and nonstretched. 64×64, 128×128, and 256×256 grid points were used. Standard discretization schemes of interFoam were applied: backward Euler in time, limited linear for the advection terms of the velocity components, and van Leer for the advection of the scalar. Interface compression (see Rusche[8]) has been used to get a sharp interface. The pressure-velocity coupling was done using the

Additional Supporting Information may be found in the online version of this article.

Correspondence concerning this article should be addressed to G. Ooms at G.Ooms@tudelft.nl.

PIMPLE scheme, with two corrector loops. The following linear solvers have been applied: preconditioned conjugate gradient for the pressure, and preconditioned biconjugate for the velocity components. On the pipe wall the no-slip condition was used. At the inflow and outflow cross-sections of the pipe a periodic boundary condition was applied, so the length of the calculation domain is equal to an integer number of wavelengths at the core-annular interface. The initial velocity distribution is set equal to the analytical solution of the Navier–Stokes equation for core-annular flow with a smooth interface. The initial interfacial surface is disturbed with a sine wave with a small specified amplitude.

Validation Against Linear Stability Calculations

In linear stability calculations of core-annular flow through a pipe one starts with a concentric, unperturbed (perfectly smooth) interface between the core and the annulus (also called PCAF). A small perturbation is then applied to the interface and the growth rate and the speed of waves at the core-annular interface is calculated (see, for instance, Li and Renardy[4]). This analysis also gives the wavelength of the fastest growing disturbance. In the comparison of our numerical simulations with the results of linear stability calculations, we choose the length of the computational domain to be equal to this wavelength. According to linear stability theory a small perturbation at the interface will grow exponentially. After a certain period a linear analysis no longer applies and the growth rate of the perturbation decreases and saturation of the growth takes place. Finally, a wave with a steady finite amplitude has developed. We define the dimensionless wave amplitude Amp as

$$\mathrm{Amp} = \frac{y_{\mathrm{crest}} - R_1}{R_1} \tag{1}$$

where R_1 is the distance between the pipe centerline and unperturbed core-annular interface position and y_{crest} the radial distance from the centerline to the wave crest. According to linear stability theory the growth rate of a perturbation is given by

$$\mathrm{Amp}\,(t) = \mathrm{Amp}\,(0)e^{\mathrm{kt}} \tag{2}$$

The time $t^\star$ has been made dimensionless in the following way $t = t^\star V_0^*(0)/R_1$. $V_0^*(0)$ is the core velocity at the centerline of the pipe for the unperturbed core-annular flow. The growth rate $k^\star$ has been made dimensionless as follows $k = k^\star R_1/V_0^*(0)$. Amp(0) is an arbitrarily chosen, very small, initial amplitude of the wave.

Growth rate and wave shape development

Li and Renardy[4] compared the results of their numerical calculations, using the VOF method, with the results of linear stability calculations for laminar core-annular flow. The case that they studied is characterized by the following values of the dimensionless groups

$$\begin{aligned} &m = 0.00166 \;\; a = 1.28 \;\; \zeta = 1.10 \;\; K = -0.454 \\ &J = 7.96e{-}2 \;\;\; Re_1 = 0.93, \end{aligned} \tag{3}$$

in which $m = \mu_w/\mu_o, a = R_2/R_1, \zeta = \rho_w/\rho_o, K = (f^* + \rho_o g)/(f^* + \rho_w g)$, $J = \sigma^* R_1 \rho_o/\mu_o^2$ and $Re_1 = \rho_o V_0^*(0) R_1/\mu_o$. $\mu_w = 0.001$ kg/ms and $\mu_o = 0.601$kg/ms represent, respectively, the dynamic viscosity of the annular liquid and the core liquid. $R_2 = 0.00476$ m is the pipe radius and $R_1 = 0.00372$ m the distance from the centerline of the pipe to the smooth (unperturbed) core-annular interface. $f^* = -9172\mathrm{kg/m^2 s^2}$ is the driving pressure gradient. $\rho_o = 905\mathrm{kg/m^3}$ and $\rho_w = 995\mathrm{kg/m^3}$ are the densities of the core liquid and annular liquid. g is the acceleration due to gravity, $\sigma^* = 8.54 \cdot 10^{-3}\mathrm{kg/s^2}$ the surface tension at the core-annular interface and $V_0^*(0) = 0.166\mathrm{m/s}$ the centerline velocity for the smooth core-annular flow. The wavelength α^* was chosen to be equal to the fastest growing wavelength found from a linear stability calculation ($\alpha^* = 0.0116$m). Li and Renardy found a value for the growth rate $k = 0.1940$ in good agreement with linear stability prediction. We repeated this calculation (for the same condition as used by Li and Renardy) to check the reliability of our numerical code (also based on the VOF method and applying periodic boundary conditions). We found the same result. The details of this study are reported in Ooms et al.[5]

We have extended this calculation by studying the influence of the initial conditions by changing these conditions while keeping the physical parameters, the computational mesh, and the time step restriction the same as in the foregoing calculation. We studied two different initial conditions. In the first one, we choose the initial dimensionless amplitude equal to 10^{-3} (in the original calculation it was 10^{-6}) and kept the wavelength the same as in the foregoing case. In the second, we choose a wave with again an initial dimensionless amplitude of 10^{-3} but a wavelength that has half the value of the foregoing one, so in that case the initial disturbance in the computational domain is two wavelengths long. The results for amplitude and interface profile are shown in Figures 1 and 2. The growth rate for the single-sine initial condition is again equal to the theoretical result of the linear stability calculation. However, the growth rate for the double-sine case is rather different, although the final amplitude is the same as for the single-sine case. During the calculation, the double-sine wave shape gradually disappears and develops into a single-sine one equal to the wave shape of the original case. This implies that the starting condition does not influence the final state of the simulation. Only the flow development is different.

Stability of PCAF

Hu et al.[6] made linear stability calculations for oil–water core-annular flow under the assumption that the densities of the liquids were equal. Due to this simplification the dimensionless numbers K and ζ become equal to 1. So no buoyancy force is present. The result of their linear stability calculation is a map for the dimensionless wave number vs. Reynolds number, in which regions of stable and unstable core-annular flow are given (see Figure 3a). We have checked the correctness of this map with five numerical simulations: two in the stable region (star symbols in the figure) and three in the unstable region (square symbols in the figure). As can be seen the results are in agreement with the linear stability calculations.

In Figure 3b more detailed results are given for one of the points ($Re_1 = 9.1$) in the stable region. For this point, we carried out simulations for three cases with increasing initial amplitude of the wave. As can be seen for all cases the wave amplitude decreases as a function of time and the final result is PCAF in agreement with the theoretical result.

In Figure 4 more detailed results are given for one of the points ($Re_1 = 182.4$) in the unstable region. We found that at first the wave shape changes from a sine into a bamboo wave (BW). Then, the amplitude starts to grow and gets the value as shown in the figure.

Based on the results of this section, we can conclude that the results of our numerical simulations are in good agreement with results of linear stability calculations. At larger

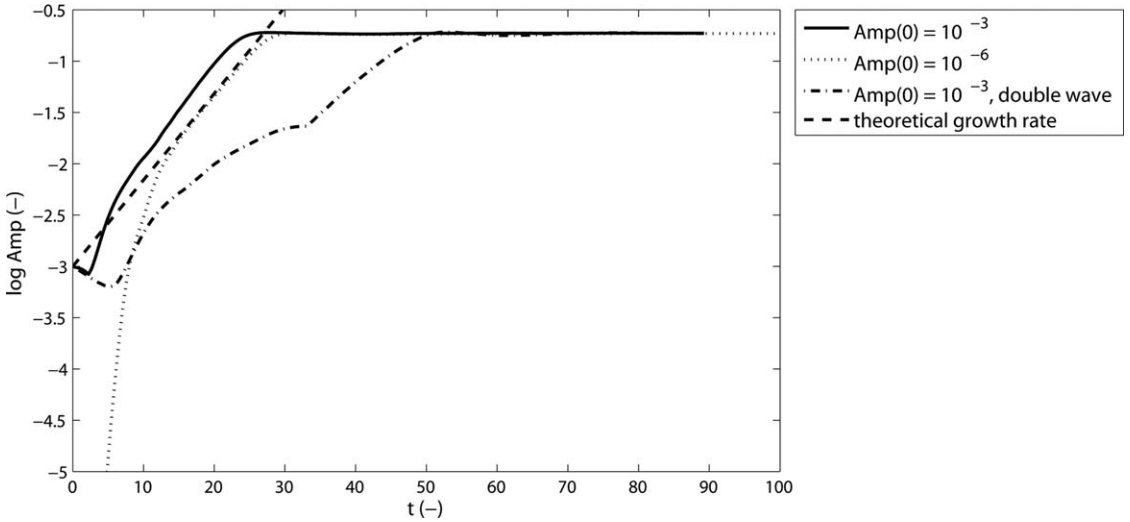

Figure 1. Growth rate characteristics for simulation with single-sine and double-sine initial wave.

wave amplitudes a saturation of the growth occurs, which can no longer be predicted by linear stability theory. Predictions by numerical calculations are then still possible.

Comparison with Experiments of Bai et al.[7]

To further check the reliability of our numerical simulations, we compared our numerical predictions with experimental results of Bai et al.[7] for laminar core-annular flow. They carried out concentric, upward, and downward, oil–water core-annular flow experiments in a vertical pipe. The experimental results for upflow are summarized in the flow pattern map shown in Figure 5. The superficial oil and water velocities are given along the axes. The superficial velocity, also called bulk velocity is equal to the flow rate divided by cross-sectional area of the entire pipe. In the map, the different flow patterns are given by BW, disturbed bamboo waves (DBW), slugs, bubbles, oil-in-water dispersion, and oil-sticks-on-the-wall. For the points given in the map the flow pattern, holdup, and pressure gradient are documented. We simulated numerically the six cases shown in Figure 5. All these cases correspond to one of the experimental points of Bai et al. For the sake of brevity, we shall discuss here only three cases (Case 1, 3, and 4 in Figure 5). The general conclusion for the other cases is the same as for the cases discussed here. The details about all points can be found in Beerens.[9]

Numerical simulation on a one-wavelength-long computational domain (Case 1)

The dimensionless numbers for this case are

$$m=0.00166\ \ a=1.28\ \ \zeta=1.10\ \ K=-0.930$$
$$J=7.9610^{-2}\ \ Re_1=2.855 \tag{4}$$

All quantities have the same value as for the Li and Renardy case discussed before. Only the pressure gradient is larger $f^*=-9303\mathrm{kg/m^2s^2}$ and hence the centerline velocity for the smooth core-annular flow is larger $V_0^*(0)=0.51\mathrm{m/s}$. In this calculation, we start again with a concentric core-annular flow with an almost constant radius of the core liquid. In the initial condition only a very small dimensionless amplitude (at the start a value of 10^{-6}) is present. The length of the

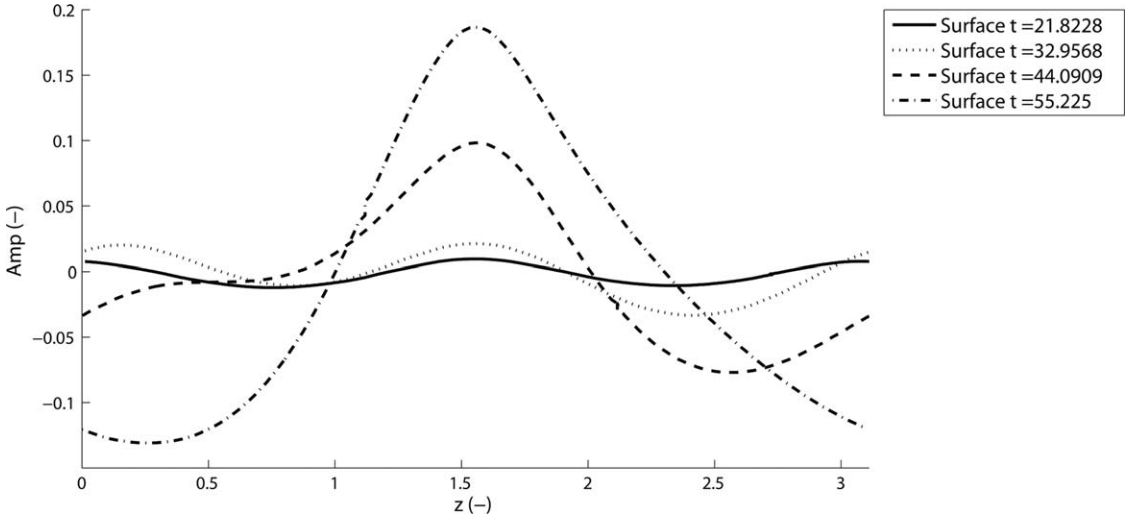

Figure 2. Development of the double-sine initial wave at different time specifications.

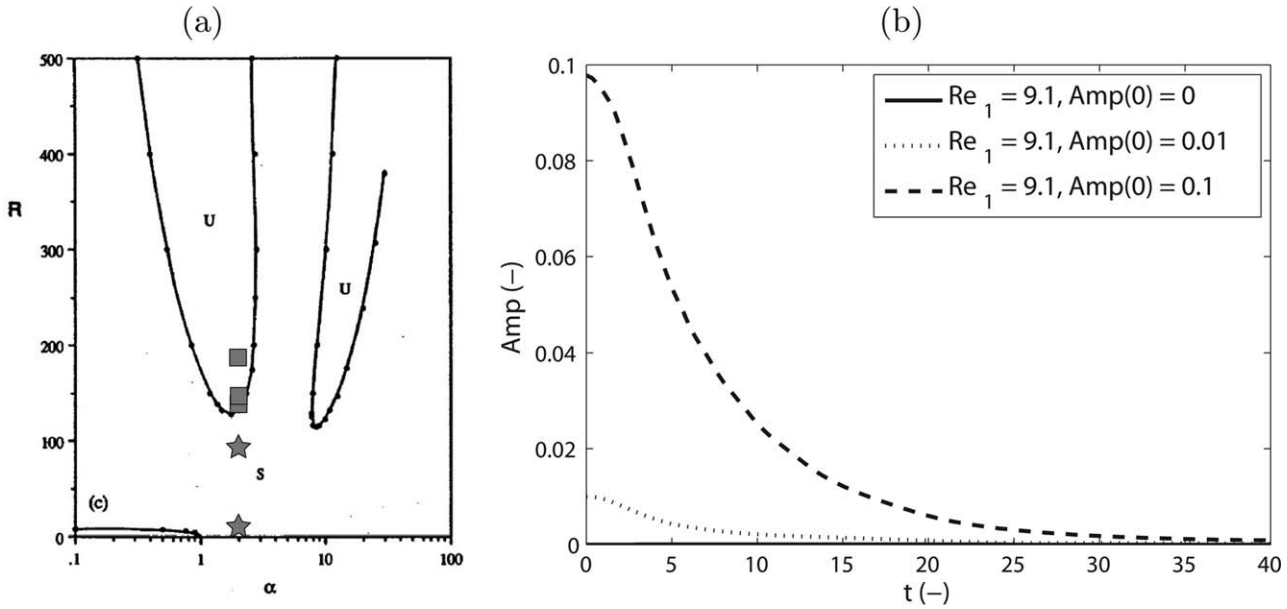

Figure 3. (a) Results from linear stability analysis reproduced from Hu et al.,[6] $m = 0.1$ and $J = 10$.

The dimensionless wave number α of Hu et al. corresponds to our $2\pi R_1/\alpha^*$. R of Hu et al. is identical to our Re_1. "U" represent an unstable region, "S" represents a stable region. The star symbols and the square symbols in the figure indicate, respectively, the stability and instability of the flow resulting from the numerical simulations. (b) Development of amplitude for one of the simulations indicated with a star symbol in (a).

computational domain is equal to the experimental value of the wavelength ($\alpha^* = 0.0116$m as documented by Bai et al.). By choosing the value of the superficial water velocity $u^*_{s,w}$ and the superficial oil velocity $u^*_{s,o}$ in the flow pattern map of Bai et al. we select the experiment (with the values for the dimensionless groups as aforementioned) that we simulate numerically. The aim of the simulation is to predict the superficial velocities of oil and water starting from the applied pressure gradient. For this simulation, we need the values of a and f^*. a (the ratio between the pipe radius and core radius) is determined from the following relation

$$a = \sqrt{1 + h \times \frac{u^*_{s,w}}{u^*_{s,o}}} \tag{5}$$

in which h is the slip ratio (defined as $h = \frac{Q_o/Q_w}{\Omega_o/\Omega_w}$, in which Q_o and Q_w are the volume flow rates of oil and water, respectively, and Ω_o and Ω_w the volumes of oil and water; In the article by Bai et al. h is called the holdup ratio). The experimental slip ratio has the value $h = 1.39$. So, we can calculate the value of a from Eq. 5 by using the experimental values of $h, u^*_{s,w}$, and $u^*_{s,o}$ and we find $a = 1.28$ (aforementioned). The pressure gradient f^* can be calculated using the following relation given by Bai et al

$$f^* = g \cdot \left(\rho_o \cdot \frac{1}{a^2} + \rho_w \cdot \left(1 - \frac{1}{a^2} \right) + \theta_e \cdot \rho_w \right) \tag{6}$$

in which the part $g\theta_e\rho_w$ is due to friction and the remaining part due to gravity. The value of θ_e has been documented for the experiments by Bai et al. in their publication. In this way, we find the value $f^* = -9303 \mathrm{kg/m^2 s^2}$ aforementioned. The initial velocity distribution in the core and annulus is chosen to be equal to the velocity distribution of PCAF, which is calculated analytically from the following equations (see Li and Renardy[4]) using the value of a and f^* (as determined according to the earlier procedure)

$$\begin{aligned} &\text{Annulus :} \\ &V(r) = [a^2 - r^2 - 2(K-1) ln(r/a)]/A \\ &\text{Core :} \\ &V(r) = 1 - mr^2 K/A \end{aligned} \tag{7}$$

in which $V(r)$ is the velocity [made dimensionless by the centerline velocity $V^*_0(0)$] as a function of the dimensionless distance r from the centerline (made dimensionless by the core radius R_1). The quantity A is equal to

$$A = mK + a^2 - 1 + 2(K-1)\ln(a) \tag{8}$$

Starting from the initial velocity distribution, we can calculate [using the applied pressure gradient (f^*) and ratio of pipe

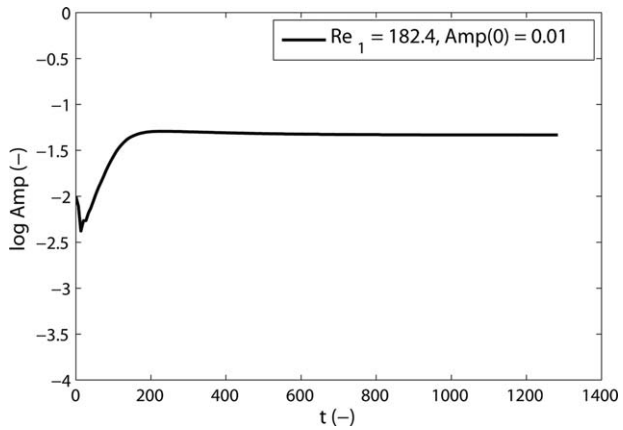

Figure 4. Development of amplitude for the simulation indicated with a square symbol in 3a.

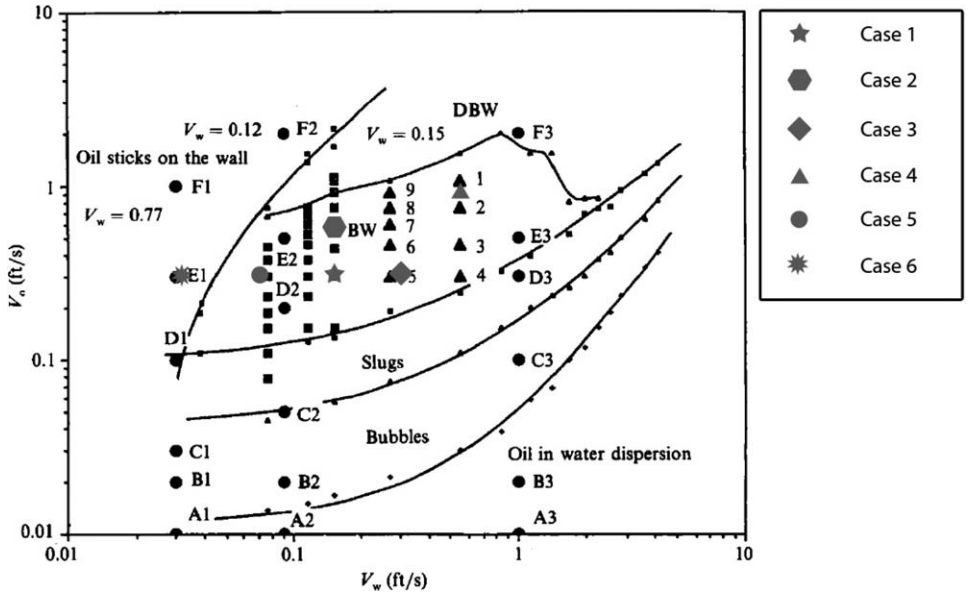

Figure 5. Map of different flow regimes according to Bai et al. (1992).

The positions of the six cases that we simulated numerically are indicated in the map. According to our nomenclature $V_o \equiv u^*_{s,o}$ and $V_w \equiv u^*_{s,w}$. Note that the superficial velocities are in ft/s.

radius and core radius (a)] the flow development for the chosen case. Our numerical results for the transient development of the superficial velocities, the slip ratio, and amplitude are given in Figure 6, the wave shape in Figure 7. The slip ratio quickly develops to its final value. As can be seen from Figure 6, the wave amplitude does not change anymore after $t = 35$. Also the wave shape shows the typical BW shape quickly and remains the same thereafter. It turns out that the development of the superficial velocities takes the longest time. The development in time of the superficial velocities can be explained in the following way: To reduce the computing time the centerline velocity $V_0^*(0)$ in the initial velocity distribution has been given a lower value than $0.51\mathrm{m/s}$, so that the initial velocity distribution is already closer to the expected final distribution found experimentally by Bai et al. Because of the lower initial velocity the pressure drop will then first accelerate the flow. Thereafter, the flow slows down due to the growth of the waves at the interface and then reaches the final state. The numerical results for the superficial velocities compare reasonably well with the experimental ones. No differences larger than 15% are found and both are lower than the experimental results. The ratio between the superficial velocities becomes constant this can also be concluded for the slip ratio. The numerically predicted slip ratio is equal to 1.45 and for the experiment it is 1.39.

The final value of the computed centerline velocity is $V_{\mathrm{end}} = 0.146\mathrm{m/s}$, whereas the centerline velocity for a smooth core-annular flow (at the same pressure drop and average *in situ* volume fraction) is $V_0^*(0) = 0.51\mathrm{m/s}$. (The value of the measured centerline velocity is $V_{\mathrm{exp}} = 0.166\mathrm{m/s}$). This shows the considerable effect of the waves on the flow properties of core-annular flow, as compared to the flow properties predicted assuming a smooth interface. This effect was found for all six cases that we studied.

For the flow domain contour plots have been made for the volume fraction of the core liquid (oil) and annular liquid (water) and for the reduced pressure (see Figure 8; The reduced pressure is equal to the total pressure minus the pressure contribution due to gravity. The reduced pressure gives the contribution to pressure due to flow and surface tension.) The volume fraction gives a clear picture of the wave shape. Also some information about the sharpness of the calculated interface can be read from the figure. The reduced pressure is varying throughout the domain, but its contours are almost everywhere horizontal in the gap between the oil and the pipe. Only close to the wave crest (where a recirculation is present) they deviate somewhat from the horizontal. So the reduced pressure at the core-annular interface can be studied by means of the related value at the pipe wall. The reduced pressure contours and the reduced pressure distribution at the pipe wall are shown in Figure 8. At the front of the wave, we see a gradual build up of the reduced pressure, while at the top it rapidly decreases.

The velocity distribution is studied in two ways. First, the velocity profile along two radial lines is studied. One line is through the wave crest and one through the wave trough. The axial velocity distributions along these two lines are given in Figure 9 for a reference system in which the wall is at rest. Next, the velocity field is studied by means of streamlines. For the analysis of the streamline pattern two different reference systems were used. In the first system, the wall has zero velocity, whereas in the second system the wave is at rest. The second system is useful to identify flow structures which travel along with the flow. The results are also shown in Figure 9. It is seen that a strong recirculation is present in the trough of the waves. In the reference system in which the wall is at rest a weak vortex is observed at the wave crest. This vortex is due to the influence of gravity. When the pressure force is smaller than the gravitational force in the annular layer, there can exist a region near the pipe wall (near the wave crest) where the velocity is negative. This effect disappears when the pressure gradient and thus the velocity is increased. The faster annular liquid flow near the interface (in the trough) is likely due to the strong recirculation region in the trough aforementioned.

Bai et al.[10] and Li and Renardy[4] derived similar results for the reduced pressure distribution and velocity distribution

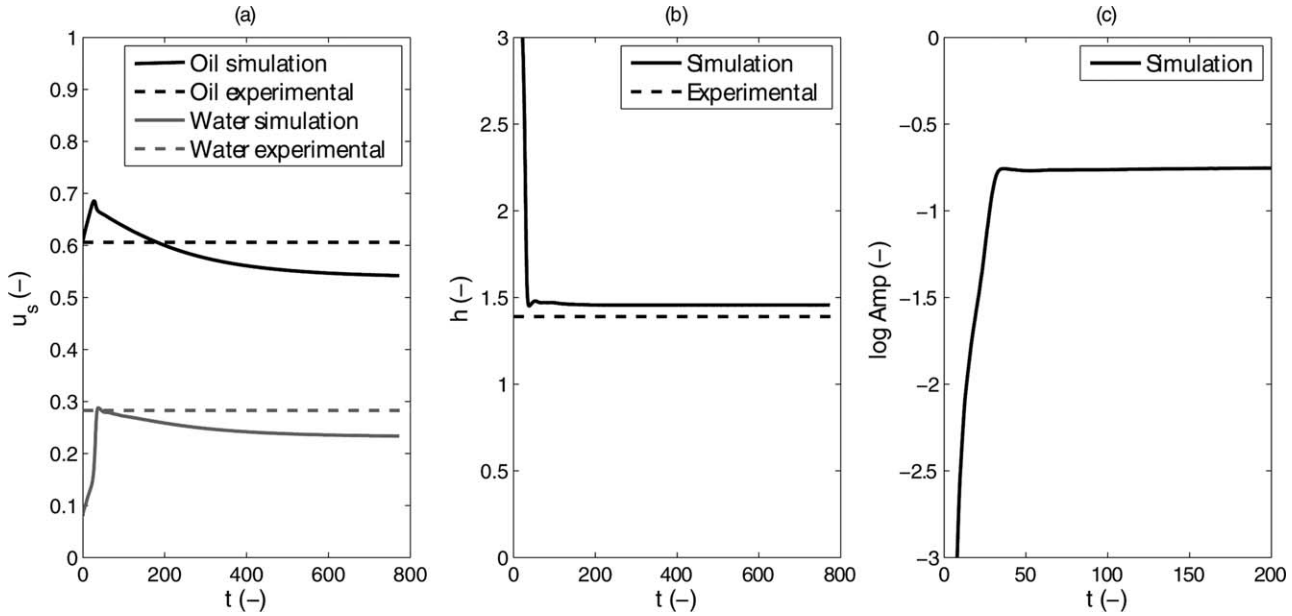

Figure 6. Comparison for Case 1 of one-wavelength-long simulation results and experimental results for (a) superficial velocities, (b) slip ratio, and (c) wave amplitude.

($u_{s,o}=u^*_{s,o}/V_{exp}$; $u_{s,w}=u^*_{s,w}/V_{exp}$; $V_{exp}=0.166\,m/s$). V_{exp} is the measured value of the centerline velocity. $V^*_0(0)=0.51\,m/s$. $V^*_0(0)$ is the centerline velocity for the smooth core-annular flow. $V_{end}=0.146\,m/s$. V_{end} is the final value of the computed centerline velocity.

as shown in Figures 8 and 9. Bai et al. assumed a solid core and density matching of the liquids in the core and annulus for their direct numerical simulation. Li and Renardy (using the volume-of-fluid method) did not have the value of the driving pressure gradient, which is necessary to make the calculation by prescribing a and f^*. Therefore, they solved the inverse problem to find the experimental result.

Long-pipe numerical simulations (Case 1)

For all simulations periodic boundary conditions were applied. This means that an integral number of wavelengths has to fit in the calculation domain. In the simulation of the Bai et al. experiment given above the length of the computational domain was equal to the experimentally found wavelength. In this section an attempt is made to calculate numerically the (most unstable) wavelength for this experiment (Case 1) and study (when it is different from the one used before) the influence on the flow development. For that purpose, the calculation for the one-wavelength-long computational domain has been repeated for a very long pipe. The region of possible wavelengths that fits in the calculation domain is then significantly larger. The length of the periodic domain used for the one-wavelength simulation is 0.0116 m, whereas for the long-pipe simulation the calculation domain has a length of 0.348 m. The dimensionless numbers for this case are again given by Eq. 4, the same as for the one-wavelength simulation. The initial wavelength and amplitude is the same as for the one-wavelength-long simulation. The results in terms of superficial velocties, slip ratio, and wave amplitude are given in Figure 10. Comparing

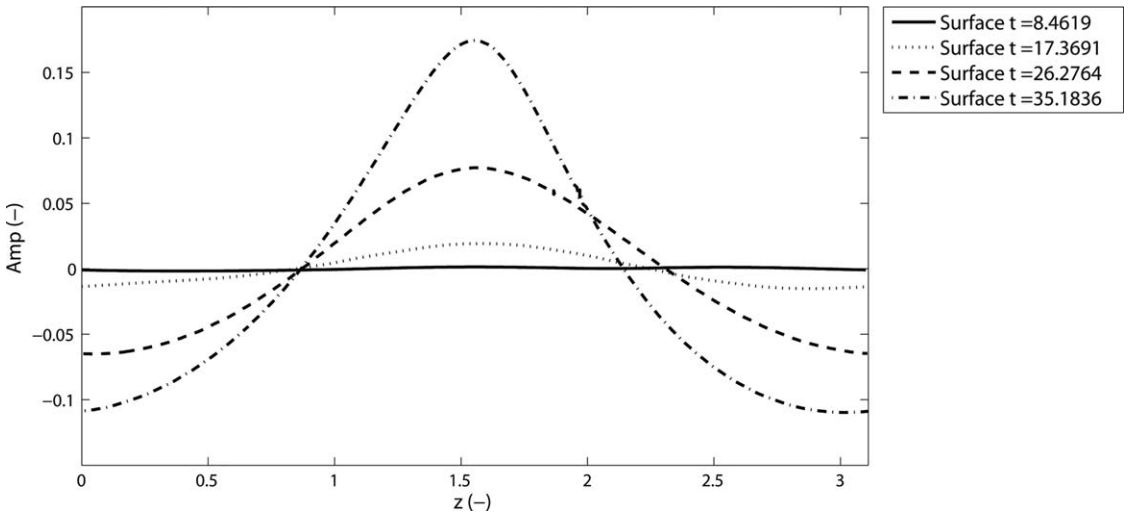

Figure 7. Interface profile at four different time instances.

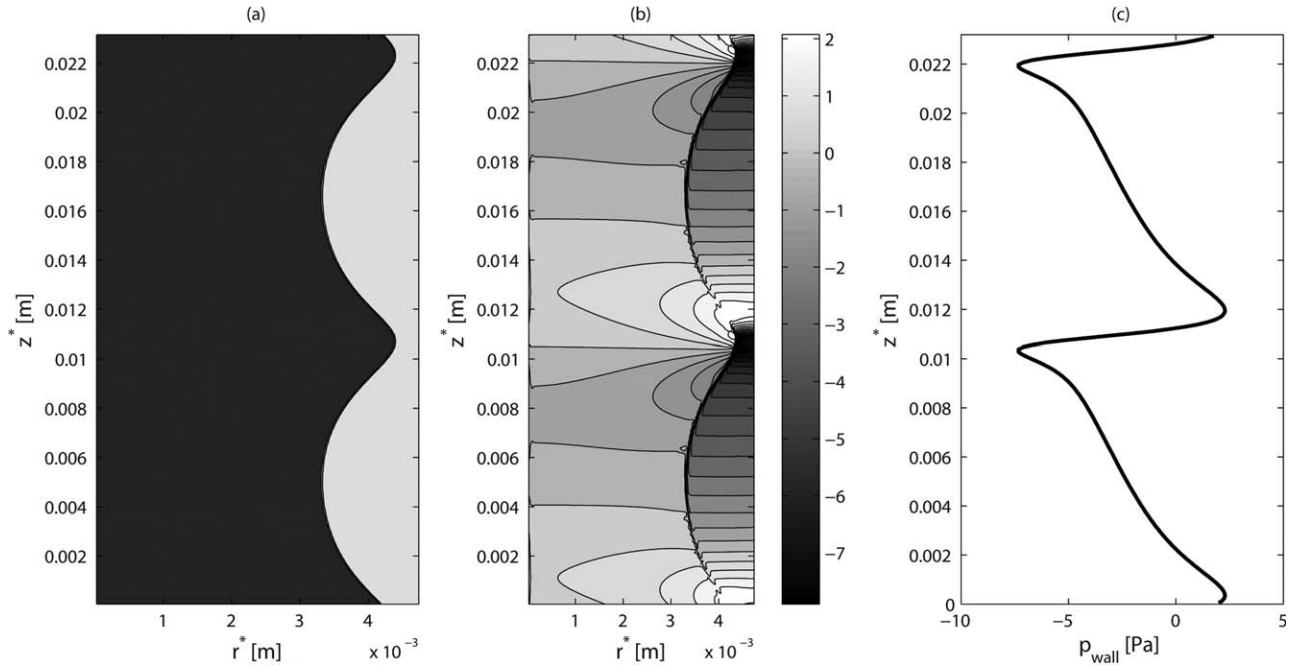

Figure 8. (a) Volume fraction (black indicates oil and gray water); (b) Reduced pressure contours; (c) Reduced pressure distribution at the wall.

these results with the one-wavelength results of Figure 6 it can be concluded that the agreement is reasonable (although the development to the final value of the superficial velocities and of the slip ratio is somewhat different). The simulation is not performed for the same physical time as for the one-wavelength case, as the computation time is much larger for the long-pipe simulation.

The interface profile at the end of the simulation is given in Figure 11. It can be seen that not a single wavelength is present but that a range of different wavelengths exists. The distance between two succeeding tops has been measured and defined as wavelength. The distribution of these wavelengths for three different time instances is given in Figure 12. The average wavelength from these results is equal to 0.0109 m, not very different from the chosen wavelength for the one-wavelength simulation. The wave amplitude depends on the wavelength (see Figure 13). The distance between the wave crest and the pipe centerline remains nearly constant,

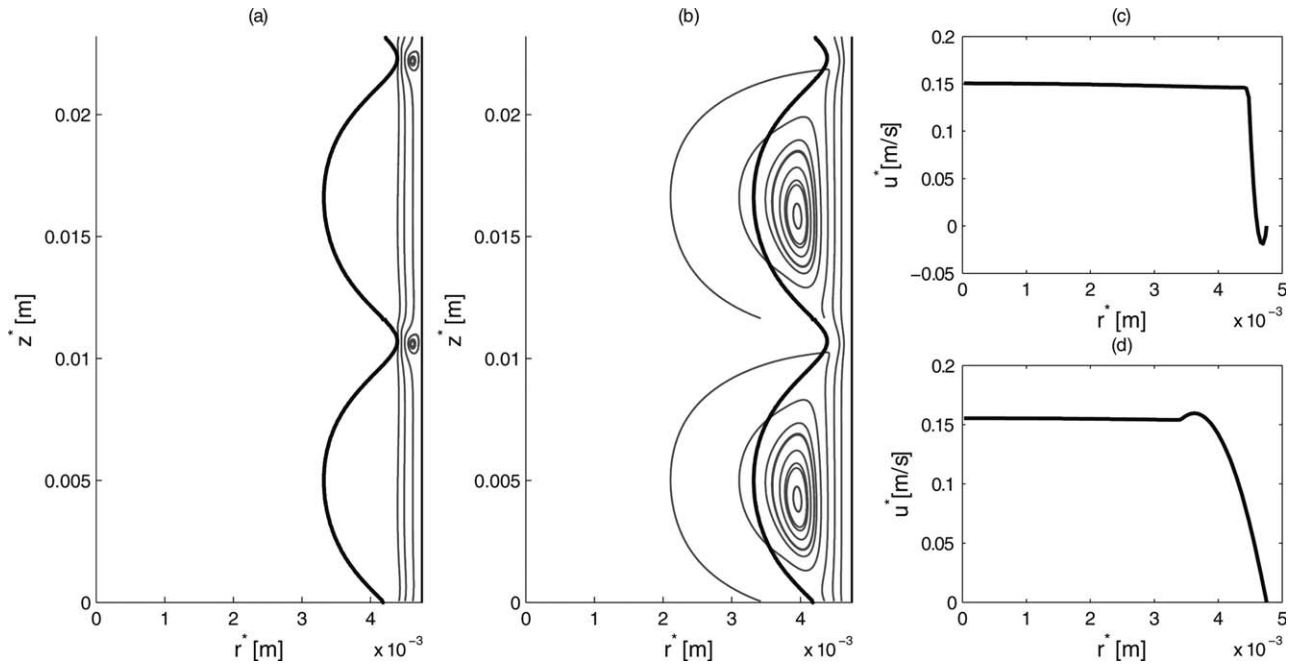

Figure 9. (a) Streamlines in a system with zero wall velocity. (b) Streamlines in a system with zero wave velocity. (c) Velocity profile for crest section. (d) Velocity profile for trough section.

The velocity profiles in (c) and (d) are for a reference system in which the wall is at rest. In this reference system, the wave velocity is 0.146 m/s.

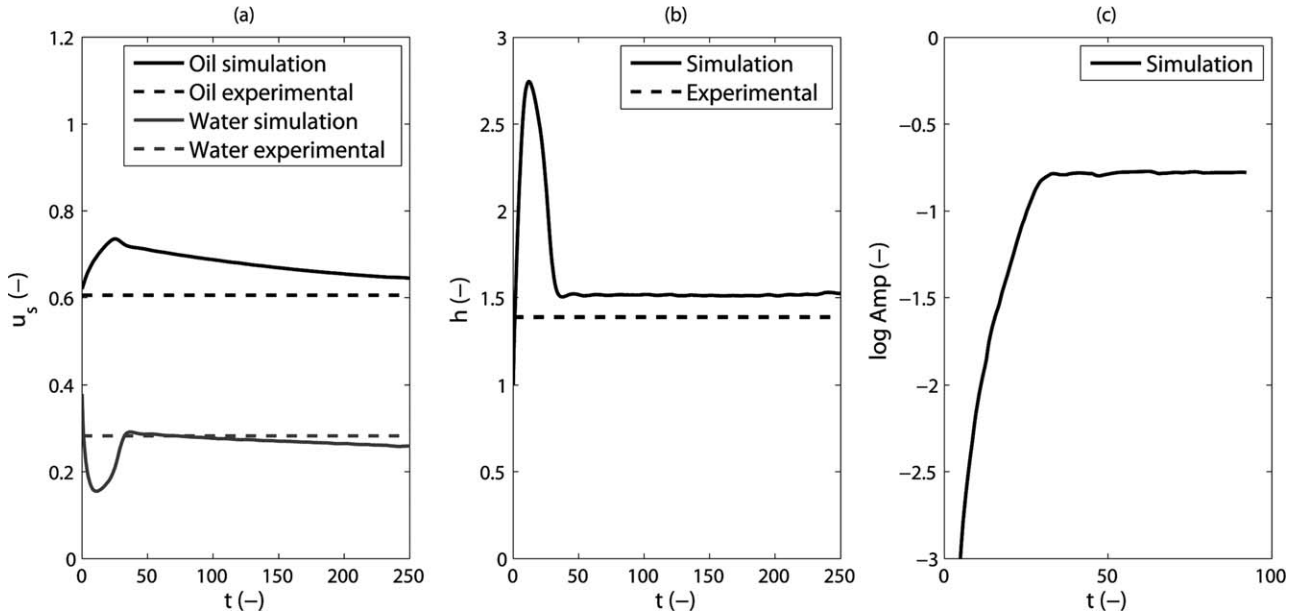

Figure 10. Comparison for Case 1 of long-pipe numerical results and experimental results for (a) superficial velocities, (b) slip ratio, and (c) wave amplitude.

whereas the distance between the wave trough and the pipe centerline decreases with increasing wavelength. So the wave trough becomes deeper for longer waves. There is one point that does not fit in the correlation. It belongs very likely to a wave that is being generated.

From a comparison between the one-wavelength-long case and the long-pipe case it can be concluded that the wavelength (distribution) has an influence on the flow development of core-annular flow. It seems that in case the flow can choose by itself its wavelength distribution (long-pipe case) the superficial velocities are somewhat larger than for the case that only one wavelength is imposed on the flow. In this context, the following remarks are made concerning the forces that are important for the core-annular flow studied earlier. The driving force for the core $(f^*+\rho_o g)$ pushes the core in an upward vertical direction, whereas this force is downward for the annular layer $(f^*+\rho_w g)$. However, there is a frictional force at the interface between the core liquid and the annular liquid, which exerts an upward force on the annular liquid and a downward one on the core liquid. The net result is that the superficial velocities for both liquids are in upward direction. With the development of interfacial waves this interaction between core and annulus increases, so that the core superficial velocity decreases and the annular superficial velocity increases. The wavelength distribution and the wave amplitude are important in this process.

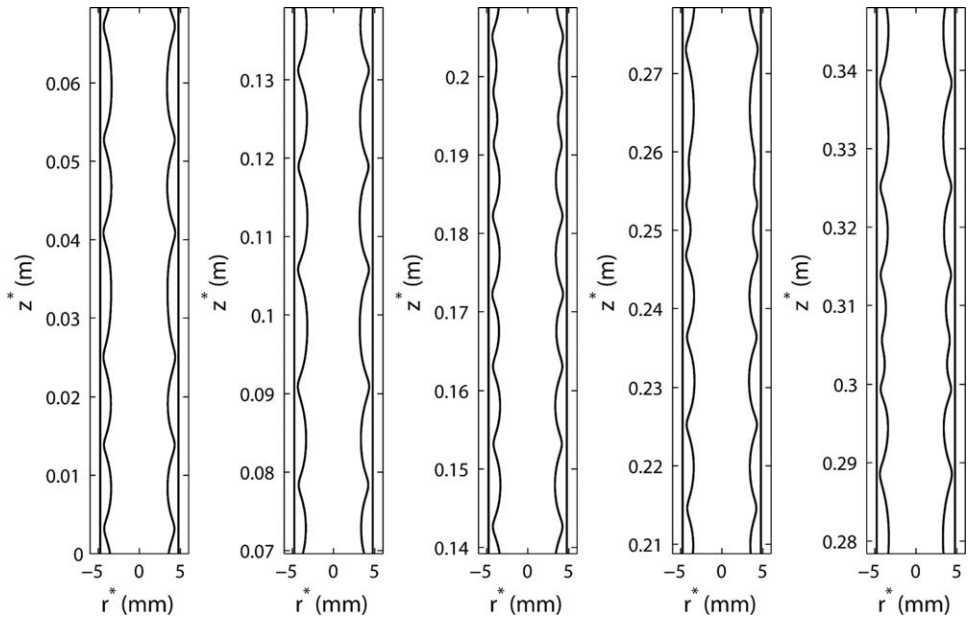

Figure 11. Interface profile as calculated with long-pipe simulation. (Please note that in the figure the pipe has been cut in five parts because of its length.)

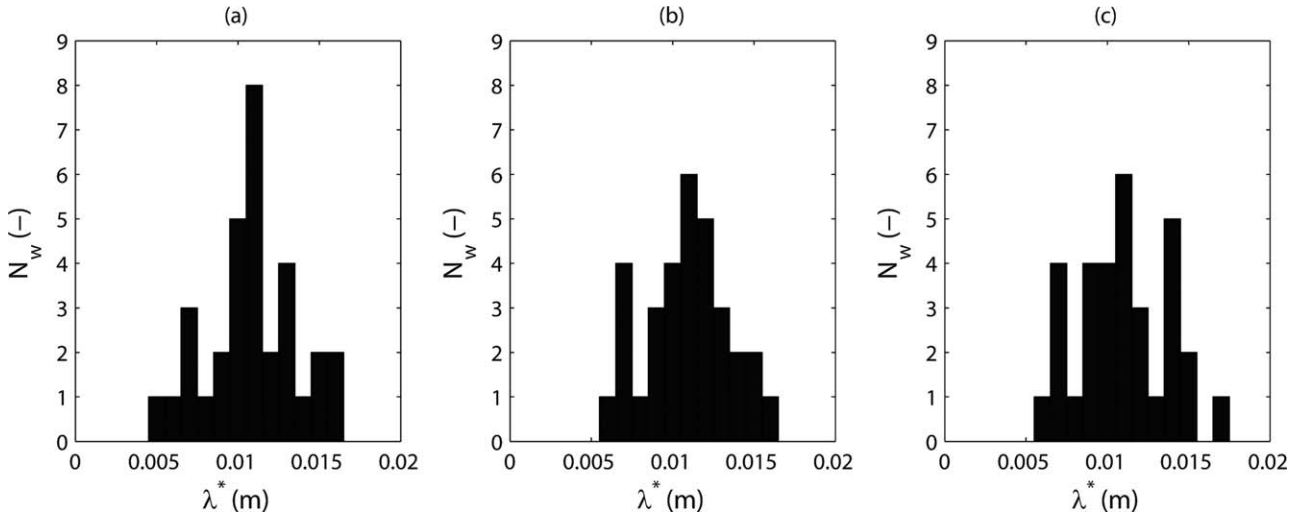

Figure 12. Wavelength distribution for (a) $t = 84$ (b) $t = 86.5$ (c) $t = 89$ (N_w = number of waves).

Numerical simulation on a one-wavelength-long computational domain (Case 3)

Rodriguez and Bannwart[11] made a stability analysis for core-annular flow based on a rigorous one-dimensional two-fluid model. One of their results is that a core-annular flow close to the "slugs" boundary (see Figure 5) has a wavelength of about twice the pipe diameter, which is considerably larger that the wavelength for a core-annular flow in the middle of the BW regime or for a DBW. We have compared this finding with a result from our calculation method for Case 3, using two different values of the wavelength. For Case 3, the superficial water velocity is twice the one for Case 1. So the water layer is much thicker than for Case 1. According to linear stability theory it has a wavelength of 0.0156 m. The dimensionless numbers for Case 3 are given by

$$m=0.00166 \;\; a=1.55 \;\; \zeta=1.10 \;\; K=-2.03$$
$$J=6.5810^{-2} \;\; Re_1=4.02 \tag{9}$$

For Case 3 two different calculations were carried out. For the first calculation a wavelength of 0.0116 m. was used, which was the most unstable wavelength (according to linear stability theory) for Case 1. For the second calculation a wavelength of 0.0156 m was used, which was the most unstable wave (according to linear stability theory) for Case 3. As can be seen in Figure 5 Case 3 is closer to the the "slugs" boundary than Case 1. So according to Rodriguez and Bannwart, we may expect that the calculation with a wavelength of 0.0156 m. is in better agreement with the experimental data than the calculation with a wavelength of 0.0116 m. The results of the calculations are given in Figures 14 and 15. The best agreement with experimental results is indeed obtained for a wavelength of 0.0156 m. So

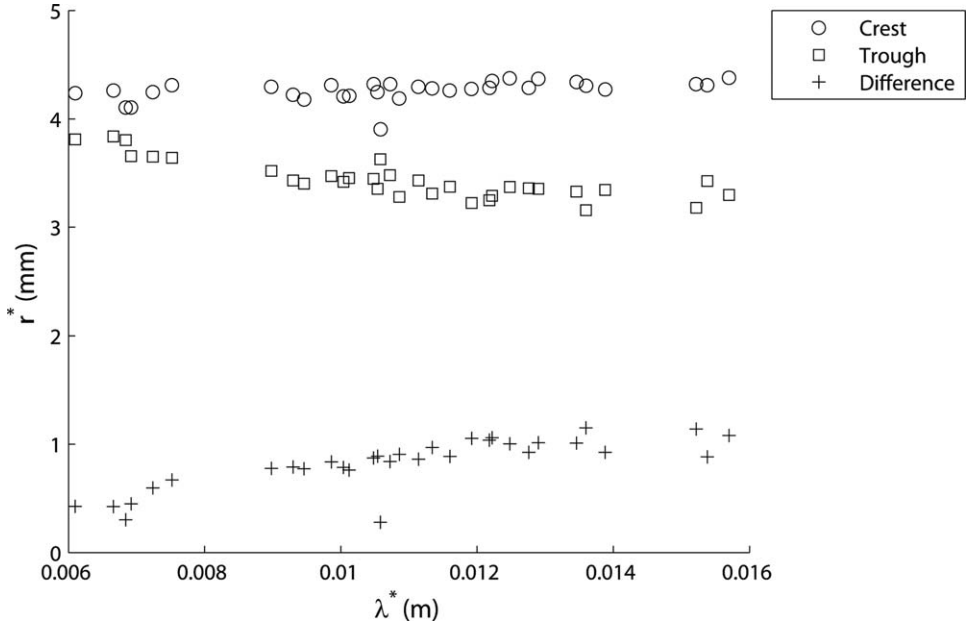

Figure 13. Relation between wave amplitude and wavelength for the long-pipe simulation of Case 1.

The distance r^* between the wave crest and the pipe centerline remains nearly constant, whereas the distance between the wave trough and the pipe centerline decreases with increasing wavelength. So the wave trough becomes deeper for longer waves.

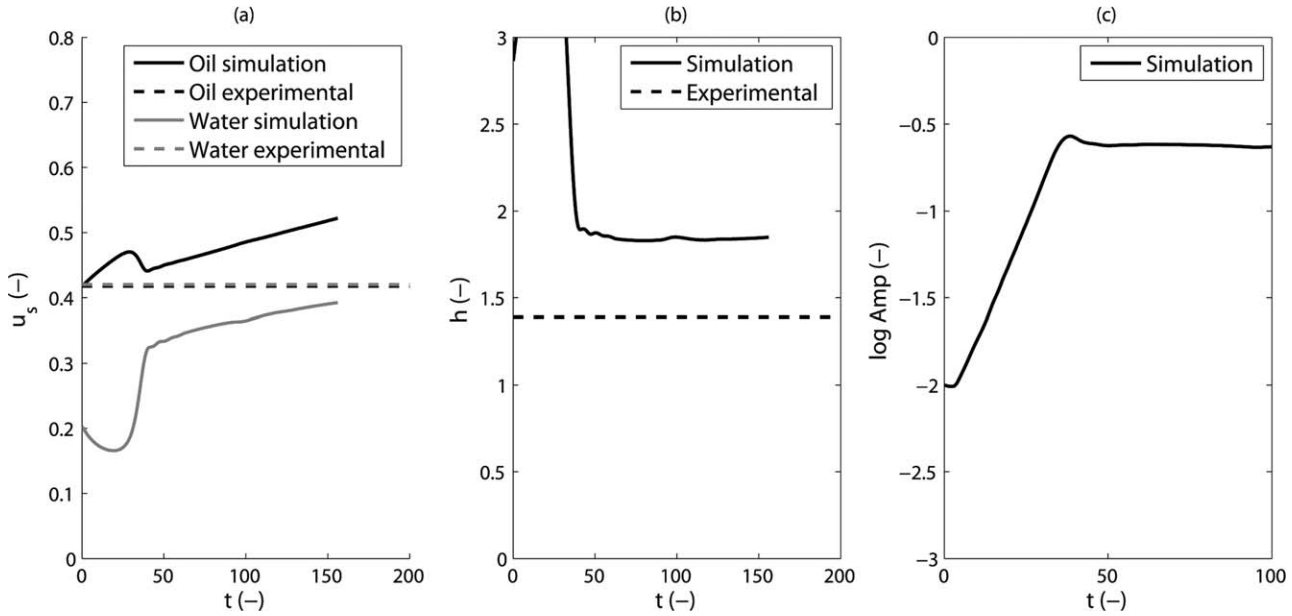

Figure 14. Comparison for Case 3 of one-wavelength-long simulation results and experimental results for (a) superficial velocities, (b) slip ratio, and (c) wave amplitude.

$(u_{s,o}=u^*_{s,o}/V_{exp}\,;u_{s,w}=u^*_{s,w}/V_{exp}\,;V_{exp}=0.240\,\mathrm{m/s}\,);V^*_0(0)=0.870\,\mathrm{m/s}$**; wavelength is 0.0116 m**

a correct choice of the wavelength (based on stability theory) is crucial.

Numerical simulation on a one-wavelength-long computational domain (Case 4)

For Case 4, the superficial oil and water velocities are increased approximately three times compared to Case 1. The dimensionless numbers for this case are given by

$$m=0.00166\;\; a=1.35\;\; \zeta=1.10\;\; K=-2.72$$
$$J=7.5110^{-2}\;\; Re_1=5.53 \qquad (10)$$

Although this case is still in the BW regime, it is close to the DBW regime as can be seen in Figure 5. We have investigated, whether that has an influence on the results. The calculation was carried out along the same lines as explained for Case 1. The results for the superficial velocities, holdup, and growth rate are given in Figure 16. The time development for Case 4 is similar to Case 1. However, the development is now much faster, and it is not reaching a steady state. It can clearly be seen that the slip ratio is varying while for Case 1 the slip ratio remained constant after saturation. This is likely due to the fact that the flow is close to the DBW regime.

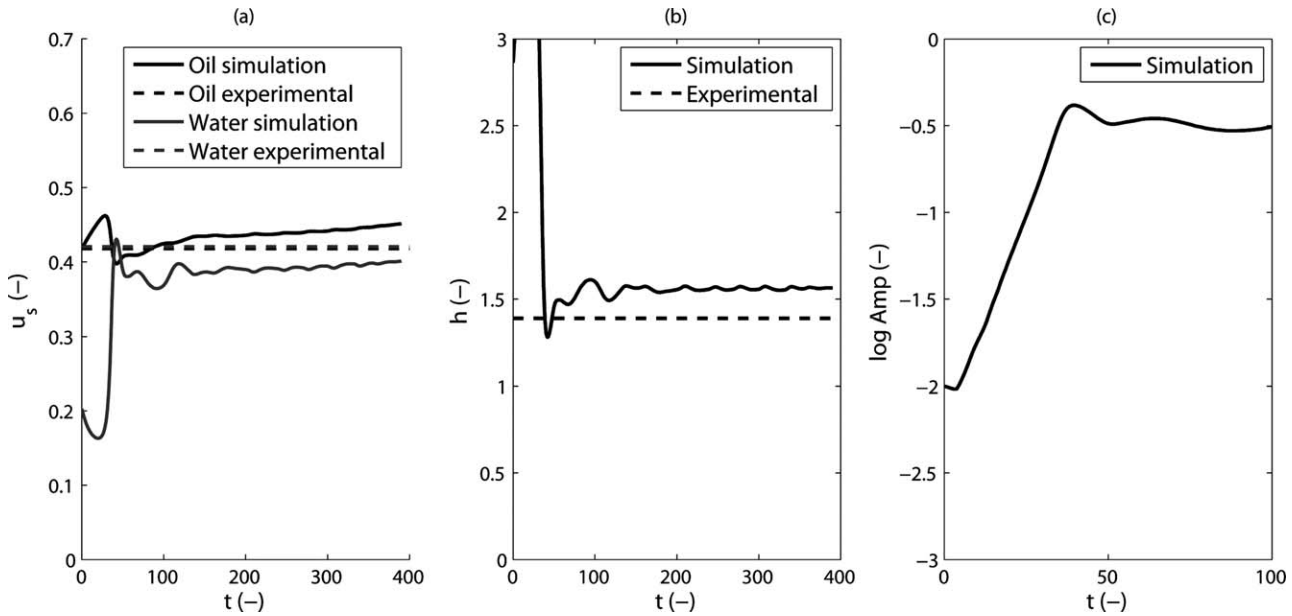

Figure 15. Comparison for Case 3 of one-wavelength-long simulation results and experimental results for (a) superficial velocities, (b) slip ratio, and (c) wave amplitude.

$(u_{s,o}=u^*_{s,o}/V_{exp}\,;u_{s,w}=u^*_{s,w}/V_{exp}\,;V_{exp}=0.240\,\mathrm{m/s}\,);V^*_0(0)=0.870\,\mathrm{m/s}$**; wavelength is 0.0156 m**

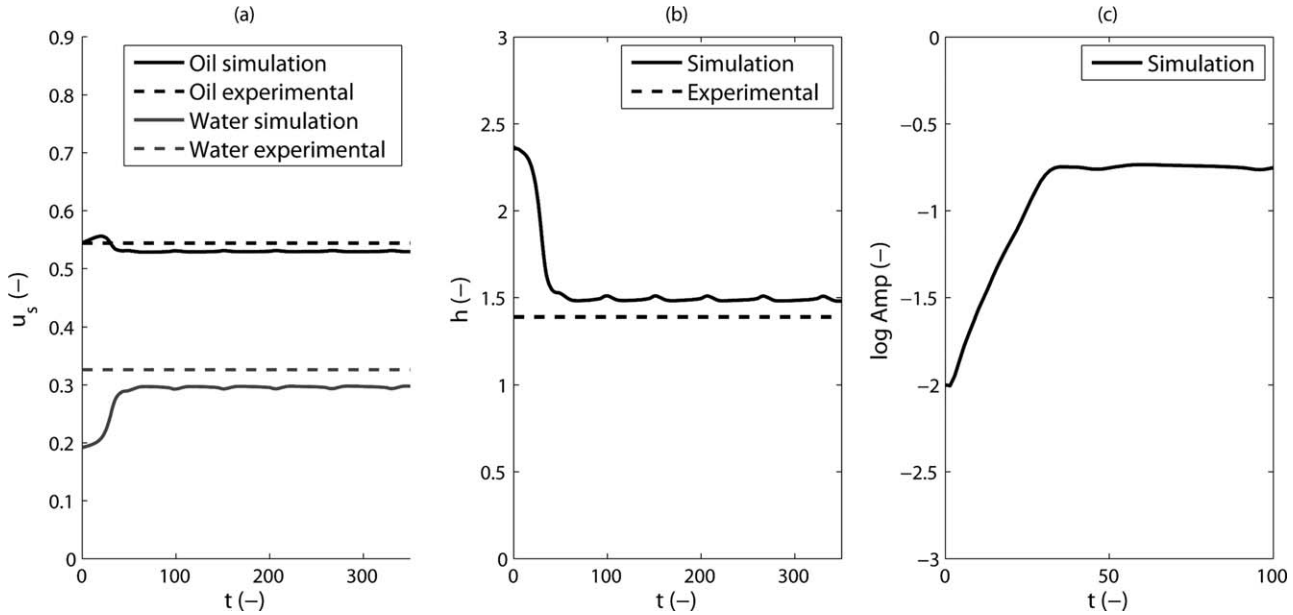

Figure 16. Comparison for Case 4 of one-wavelength-long simulation results and experimental results for (a) superficial velocities, (b) slip ratio, and (c) wave amplitude.

$(u_{s,o}=u^*_{s,o}/V_{exp}\,;u_{s,w}=u^*_{s,w}/V_{exp}\,;V_{exp}=0.51\,\mathrm{m/s}\,);V^*_0(0)=1.041\,\mathrm{m/s}\,V_{end}=0.495\,\mathrm{m/s}.$

Conclusions

The general conclusion of our study is that it is very well possible to simulate laminar core-annular flow through a pipe using the volume-of-fluid method. Predictions (for the wave shape, growth rate of the wave, stability, slip ratio, etc.) made with this method are in good agreement with theoretical results from linear stability theory and with experimental results. As periodic boundary conditions are applied, the length of the computational domain in axial direction is equal to an integer number of wavelengths of the interfacial wave. At first the length of the computational domain was chosen to be equal to the wavelength found from a linear stability calculation or from experiment. Later an estimate of the wavelength was made via long-pipe simulations. We then found that not a single wavelength occurs but a distribution of wavelengths that keeps varying as a function of time. The average wavelength is in reasonable agreement with the wavelength found from a linear stability calculation or from experiment.

We found that the effect of the waves on the flow properties of core-annular flow, as compared to the flow properties predicted assuming a smooth interface is considerable. Moreover, as shown, the calculated flow properties (for instance superficial velocities and slip ratio) for core-annular flow with waves compare well with experimental data.

There is another important reason to take into account the presence of the interfacial waves. As shown by Ooms et al.[5] the waves can generate a downward force (due to a pressure buildup at the top of the pipe) that counterbalances the upward buoyancy force in horizontal core-annular flow in case of a smaller density of the core liquid than the density of the annular liquid, thus making a stationary flow possible. In that case, the core will get an eccentric position in the pipe due to the buoyancy force and the waves will become less symmetric in the longitudinal direction of the pipe and also nonaxisymmetric (for more details see Ooms et al.[5]).

The numerical simulation of core-annular flow with a turbulent annulus and a wavy interface using the volume-of-fluid method in combination with a turbulence model is the next step in our research. We plan to study this topic in detail.

Literature Cited

1. Joseph DD, Renardy YY. *Fundamentals of Two-Fluid Dynamics, Part II: Lubricated Transport, Drops and Miscible Liquids*. New York: Springer-Verlag, 1993.
2. Oliemans RVA, Ooms G. Core-annular flow of oil and water through a pipeline. In: Hewitt GF, Delhaye JM, Zuber N, editors. *Multipase Science and Technology*, Vol. 2. Washington: Hemisphere, 1986.
3. Joseph DD, Bai R, Chen KP, Renardy YY. Core-annular flows. *Annu Rev Fluid Mech.* 1997;29:65–90.
4. Li J, Renardy YY. Direct simulation of unsteady axisymmetric core-annular flow with high viscosity ratio. *J Fluid Mech.* 1999;391:123–149.
5. Ooms G, Pourquie MJBM, Beerens J. On the levitation force in horizontal core-annular flow with a large viscosity ratio and small density ratio. *Phys Fluids.* 2013;25:032102:1–16.
6. Hu H, Lundgren S, Joseph D. Stability of core-annular flow with very small viscosity ratio. *Phys Fluids.* 1990;2(11):1945–1954.
7. Bai R, Chen K, Joseph DD. Lubricated pipelining: stability of core-annular flow. Part 5: experiments and comparison with theory. *J Fluid Mech.* 1992;240:97–132.
8. Rusche H. Computational fluid dynamics of dispersed two-phase flow at high phase fractions. PhD dissertation, Imperial College of Science, Technology and Medicine. 2002.
9. Beerens JC. Lubricated transport of heavy oil. Thesis MEAH-272 of the 3mE-Faculty of the Technological University Delft. May 2013. (Available at request from G. Ooms, g.ooms@tudelft.nl).
10. Bai R, Kelkar K, Joseph DD. Direct simulation of interfacial waves in a high-viscosity-ratio and axisymmetric core-annular flow. *J. Fluid Mech.* 1996;327:1–34.
11. Rodriguez OMH, Bannwart AC. Stability analysis of core-annular flow and neutral stability wave number. *AIChE J*. 2008;54:20–31.

Manuscript received Dec. 15, 2013, and revision received Apr. 2, 2014.